national accelerator laboratory

TM-218
2251

TARGETS FOR THE NEUTRINO BEAM; CONCEPTS

M. L. Stevenson
Lawrence Radiation Laboratory

February 15, 1970

Operated by Universities Research Association Inc. Under Contract with the United States Atomic Energy Commission

TABLE OF CONTENTS

TM-218
2251

TARGETS FOR THE NEUTRINO BEAM; CONCEPTS

M. L. Stevenson
Lawrence Radiation Laboratory

February 15, 1970

I. INTRODUCTION

The purpose of this note is to study the effects of the multiple interactions of the incident nucleon within the target in order to obtain an understanding of how this might influence the choice of the other parameters of the neutrino beam.

At NAL energies, 100 to 500 GeV, the nucleon retains on the average two thirds of its original energy. It remains an effective producer of useful energetic mesons after several interactions. The multiple interactions of a meson, on the other hand, are not useful for yielding energetic neutrinos because of the meson's much larger inelasticity ($\approx 4/5$). For this reason we have ignored the interacting meson and its production products.

In Section II the distribution of the "νth generation" nucleon interactions is calculated. A discussion of the nucleon inelasticity is given in Section III. Meson absorption in the target is considered in Section IV. A summary of the optimum target thicknesses for both low-energy and high-energy neutrino beams is presented. An estimate of the beam power dissipated in the target is also given. How a complex

nucleus itself acts like a thick target leads to a clarification of what kinds of target materials should be used in the neutrino beam target. This is treated in Section V. Finally, in Section VI some conclusions and recommendations are made in support of a two-stage neutrino-beam facility so as to best accommodate the wide energy range of the 100 to 500 GeV NAL accelera

II. A. DISTRIBUTION OF νth-GENERATION INTERACTIONS ALONG THE TARGET AXIS

One can derive the depth distribution of a given generation of nucleon by the same methods used in obtaining the daughter, grand-daughter, etc; activities in radioactive decay. Here,we assume that the interaction mean free path is independent of energy and that all interactions occur on axis. This is equivalent to the radioactivity case of equal mean lives of all generations. The incident protons, the 0th generation, are the analogue of the parents. They die off exponentially as they proceed into the target,

$$dN^{(o)}(x) = -N^{(o)}(x)\ \frac{dx}{\lambda}\ , \tag{1}$$

$$N^{(o)}(x) = N_0 e^{-x/\lambda}\ . \tag{2}$$

The 1st generation is obtained as follows:

$$dN^{(1)}(x) = \underbrace{\left[N^{0}(x) = N_0 e^{-x/\lambda}\right]\frac{dx}{\lambda}}_{\text{births}} - \underbrace{N^{(1)}(x)\,\frac{dx}{\lambda}}_{\text{deaths}} , \qquad (3)$$

$$\frac{dN^{(1)}(x)}{dx} + \frac{N^{(1)}(x)}{\lambda} = N_0 e^{-x/\lambda} \qquad (4)$$

The general solution of the ordinary differential equation,

$$\frac{dy}{dx} + p(x)y = q(x) , \qquad (5)$$

is

$$y = e^{-\int p(x)\,dx} \int e^{\int p(x)\,dx}\, q(x)\,dx + C e^{-\int p(x)\,dx} , \qquad (6)$$

where C is the constant of integration. Using Eq. (6) one finds:

$$N^{(1)}(x) = N_0 \frac{x}{\lambda} e^{-x/\lambda} , \qquad (7)$$

and writing expressions like (3) for the other generations one obtains,

$$N^{(2)}(x) = \frac{N_0}{2} \left(\frac{x}{\lambda}\right)^2 e^{-x/\lambda} , \qquad (8)$$

and in general,

$$N^{(\nu)}(x) = \frac{N_0}{\nu!} \left(\frac{x}{\lambda}\right)^{\nu} e^{-x/\lambda} , \qquad (9)$$

as the expression for the number of νth generation nucleons at the position x in the target.

Figure 1 displays the variation of $N^{(\nu)}(x)/N_0$ with x/λ for $\nu = 0$, 1, 2, and 3. The sum over all generations at a fixed position in the target yields

$$\sum_{\nu=0}^{\infty} N^{(\nu)}(x) = N_0 e^{-x/\lambda} \left[\sum_{\nu=0}^{\infty} \frac{1}{\nu!} \left(\frac{x}{\lambda}\right)^{\nu} = e^{x/\lambda} \right] = N_0, \qquad (10)$$

a value independent of x. The meaning of this result is obvious when it is realized that one is summing mutually exclusive probabilities. This is equivalent to stating that there is unit probability of finding the nucleon passing position x in some form or other.

B. Total Number of νth Generation Interactions Versus Target Length

For a target of given length, ℓ, one can determine what fraction of all interactions are of the νth generation. Integrating Eq. (9) one finds,

$$N_{\ell}^{(\nu)} = \int_0^{\ell} N^{(\nu)}(x) \frac{dx}{\lambda}$$

$$= N_0 \left\{ 1 - \left[1 + \frac{\ell}{\lambda} + \frac{1}{2!}\left(\frac{\ell}{\lambda}\right)^2 + \ldots + \frac{1}{(\nu-1)!}\left(\frac{\ell}{\lambda}\right)^{\nu-1} \right] e^{-\ell/\lambda} \right\}. \qquad (11)$$

Figure 2 shows the fractions, $N_{\ell}^{(\nu)}/N_0$, as a function of target thickness, ℓ/λ, for the first four generations.

III. NUCLEON INELASTICITY

For conceptual purposes we shall assume the nucleon inelasticity to be small and constant. Some justification for this approximation can be seen in the prediction of the Adair Model.[1] The following sketch shows his predictions compared with the measured value, the cross.

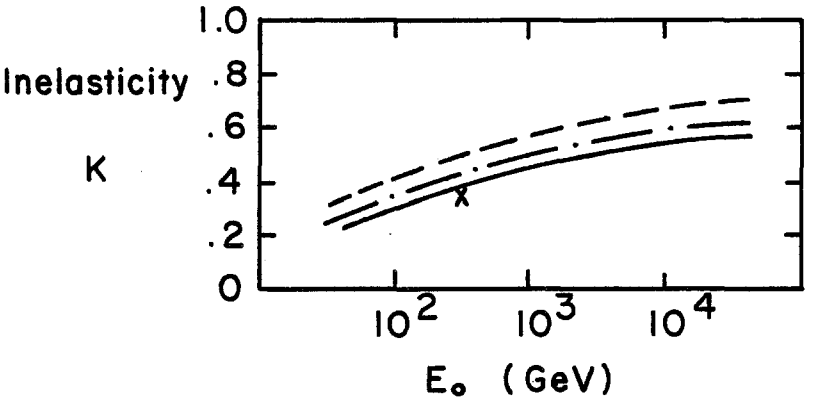

The energy of the νth generation protons is

$$E^{\nu}_{\text{proton}} = (1 - K)^{\nu} E_0 . \qquad (12)$$

The previous thick target calculations[2] for a 2.5 meter Be target (λ = 0.9 m) considered only the 0th generation interactions. From Fig. 2 we have 0.94 N_0 0th generation interactions, 0.77 N_0, 0.52 N_0, and 0.31 N_0 for the 1st, 2nd, and 3rd generations, respectively. By using the simple mnemonic[3] that the typical meson has nearly the same velocity as the incident nucleon then one estimates the following typical neutrino energies:

$$E^{\nu}_{\text{neutrino}}(\text{from pions}) \approx \left(\eta^{(\nu)}_{\text{proton}} \approx \frac{E^{\nu}_{\text{proton}}}{M_n = 1} \right) \left(q_{\pi \to \mu\nu} = 0.03\,\text{GeV} \right). \quad (13)$$

For K = 1/3

ν =	0	1	2	3
$E^{(\nu)}_{\text{prot}}$ =	200	133	89	59
$E^{\nu}_{\text{neutrino}}$ =	6	4	2.7	1.8
νth fractions =	0.94	0.77	0.52	0.31

By representing the respective neutrino distributions as delta functions, the thick target spectrum would look like the following sketch.

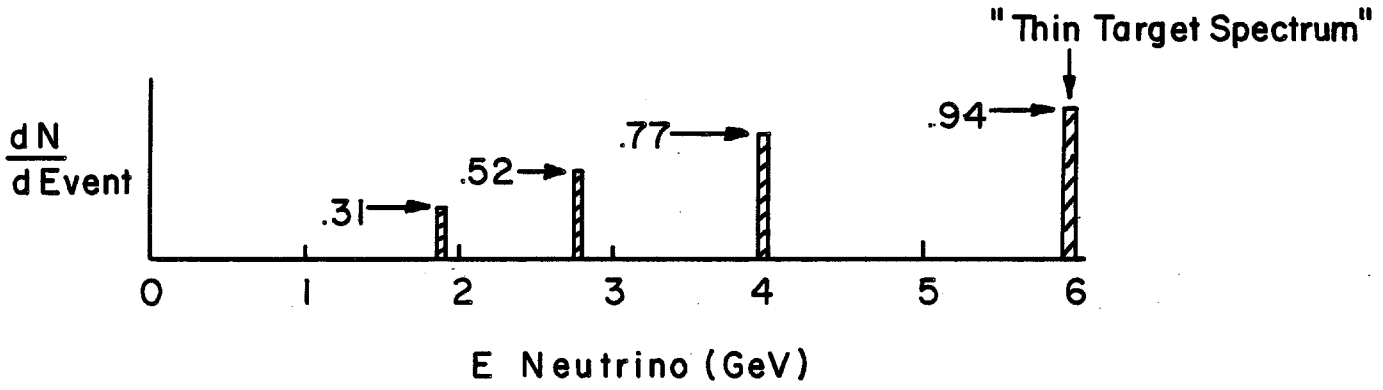

IV. MESON ABSORPTION IN THE TARGET

In this section we attempt to estimate the yields taking into account the absorption of mesons in the target. Here we shall not worry about how the meson production spectrum would be distorted by a complex nucleus. From the following sketch we separate the mesons into those that pass out the sides of the target and those out the end.

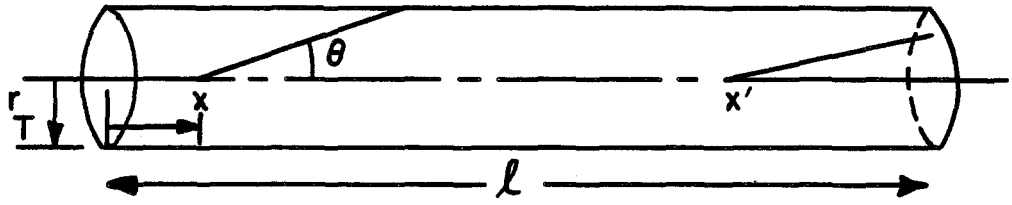

$$\frac{d^2 n_{\pi}^{(\nu)}}{dp\, d\Omega\, dx} = \frac{1}{\nu!}\left(\frac{x}{\lambda}\right)^{\nu} \frac{e^{-x/\lambda}}{\lambda}\; e^{-r_T/\theta\lambda_{\pi}}\; \frac{d^2 n^{(\nu)}}{dp\, d\Omega}\,, \tag{14}$$

for those that pass out the edge and

$$\frac{d^2 n^{(\nu)}}{dp\, d\Omega\, dx} = \frac{1}{\nu!}\left(\frac{x}{\lambda}\right)^{\nu} \frac{e^{-x/\lambda}}{\lambda}\; e^{-(\ell - x)/\lambda_{\pi}}\; \frac{d^2 n^{(\nu)}}{dp\, d\Omega}\,, \tag{15}$$

for those that pass out the end.

Summing over all generations one obtains,

$$\frac{d^2 n}{dp\, d\Omega\, dx} = \sum_{\nu=0}^{\infty} \frac{1}{\nu!}\left(\frac{x}{\lambda}\right)^{\nu} \frac{e^{-x/\lambda}}{\lambda}\; \frac{d^2 n^{(\nu)}}{dp\, d\Omega} \begin{cases} e^{-r_T/\theta\lambda_{\pi}} & \text{for } 0 < x < \ell - \dfrac{r_T}{\theta} \quad (16a) \\ e^{-(\ell - x)/\lambda_{\pi}} & \text{for } \ell - \dfrac{r_T}{\theta} < x < \ell \quad (16b) \end{cases}$$

Here, one could allow the computer to take over, inserting for $d^2 n^{(\nu)}/dp\, d\Omega$ the values given by various production models. It is possible for some simple cases to obtain exact solutions without using the full computer program.

We shall use the CKP production model for its functional simplicity. Here, we review its characteristics.

$$\frac{d^2n^{(\nu)}}{dp\,d\Omega} = \frac{n_\pi^{(\nu)}\,T_{(\nu)}}{2\pi p_0^2}\left(\frac{p}{T_{(\nu)}}\right)^2 e^{-p/T_{(\nu)}}\, e^{-p\theta/p_0} \tag{17}$$

where,

$$n_\pi^{(\nu)} = (n_0 = 0.45)\, E_{(\nu)}^{1/4}$$

$$T_{(\nu)} = (\tau_0 = 0.305)\, E_{(\nu)}^{3/4} \tag{18}$$

$$E_{(\nu)} = (1 - K)^\nu E_0, \text{ with } K \approx \frac{1}{3}\ .$$

Integrating over θ one obtains

$$\frac{d^2n^{(\nu)}}{dp} = \frac{n_\pi^{(\nu)}}{T_{(\nu)}}\, e^{-p/T_{(\nu)}}, \tag{19}$$

and finally over p to obtain,

$$n^{(\nu)} = n_\pi^{(\nu)}\ .$$

A. Large Radius Target

For this case we consider all mesons to exit the end of the target, thereby, we consider only Eq. (16b). We insert (19) into (16b) to obtain

$$\frac{d^2n}{dp\,dx} = \sum \frac{1}{\nu!}\left(\frac{x}{\lambda}\right)^\nu \frac{e^{-x/\lambda}}{\lambda}\ \frac{n_\pi^{(\nu)}}{T_{(\nu)}}\, e^{-p/T_{(\nu)}}\, e^{-(\ell - x)/\lambda_\pi}. \tag{20}$$

One could assume a perfect focusing device to cause all mesons to point at the center of the detector. The contribution from the entire target is

$$\frac{dn}{dp} = e^{-\ell/\lambda_\pi} \sum_{\nu=0}^{\infty} \frac{1}{\nu!} \int_0^{\ell} \left(\frac{x}{\lambda}\right)^{\nu} \frac{e^{-x/\lambda\left(1-\frac{\lambda}{\lambda\pi}\right)}}{\lambda} \frac{n_\pi^{(\nu)}}{T_{(\nu)}} e^{-p/T_{(\nu)}} dx \,. \qquad (21)$$

The following relationship will be useful

$$\sum_{\nu=0}^{\infty} \frac{1}{\nu!} \int_0^{t_0} t^{\nu} e^{at} dt = \frac{e^{(a+1)t_0} - 1}{a+1} \,. \qquad (22)$$

The derivation of this convenient relation is obtained by interchanging Σ and $\int$, performing the sum

$$\int_0^{t_0} \left(\sum_{\nu=0} \frac{1}{\nu!} t^{\nu} = e^{t} \right) e^{at} dt = \frac{e^{(a+1)t_0} - 1}{a+1} \,.$$

1. Total Number of Mesons from a Large Radius Target

Integrating (21) over p one obtains

$$n = e^{-\ell/\lambda_\pi} n_0 E_0^{1/4} \sum_{\nu=0}^{\infty} \frac{1}{\nu!} \int_0^{\ell} \left(\frac{x}{\lambda}\right)^{\nu} (1-K)^{\nu/4} e^{-\frac{x}{\lambda}\left(1-\frac{\lambda}{\lambda_\pi}\right)} \frac{dx}{\lambda} \,. \qquad (23)$$

Let $\beta \equiv (1-K)^{1/4}$, and regroup terms

$$\frac{n}{n_0 E_0^{1/4}} = \frac{e^{-\ell/\lambda_\pi}}{\beta} \left(\sum_{\nu=0}^{\infty} \frac{1}{\nu!} \int_0^{t_0} t^\nu e^{at}\, dt = \frac{e^{(a+1)t_0} - 1}{a+1} \right) \quad (24)$$

where

$$t = \frac{\beta x}{\lambda}\ ,\quad t_0 = \frac{\beta \ell}{\lambda}\ ,\quad a = -\frac{\left(1 - \frac{\lambda}{\lambda_\pi}\right)}{\beta}\ ,$$

$$\left[a + 1 = 1 - \frac{(1 - \lambda/\lambda_\pi)}{\beta} \right] \left(t_0 = \frac{\beta \ell}{\lambda} \right) = \frac{\ell}{\lambda}\, \beta \left[1 - \frac{\left(1 - \frac{\lambda}{\lambda_\pi}\right)}{\beta} \right] .$$

(a) <u>For $\lambda = 2/3\ \lambda_\pi$</u>, namely for a hydrogen target, where the quark model prediction is used, one obtains,

$$a = -\frac{1}{3}\,\beta\ ,\quad \left(1 + a = 1 - \frac{1}{3\beta}\right)\left(t_0 = \frac{\beta \ell}{\lambda}\right)$$

$$= \frac{3\beta - 1}{3}\ \frac{\ell}{\lambda} = \left(\beta - \frac{1}{3}\right)\frac{\ell}{\lambda}\ ,$$

$$\frac{n}{n_0 E_0^{1/4}} = \frac{3 e^{-\frac{2\ell}{3\lambda}}}{(3\beta - 1)} \left[e^{\left(\beta - \frac{1}{3}\right)} - 1 \right] . \quad (25)$$

(b) <u>For $\lambda = \lambda_\pi$</u>, with $a = 0$, $(1 + a = 1)$ $(t_0 = \beta \ell/\lambda)$,

$$\frac{n}{n_0 E_0^{1/4}} = \frac{e^{-\ell/\lambda}}{\beta}\left(e^{\beta\ell/\lambda} - 1\right) \tag{26}$$

Figure 3 displays both $\lambda = 2/3\ \lambda_\pi$, and $\lambda = \lambda_\pi$ examples of $n/n_0 E_0^{1/4}$.

2. Average Meson Momentum from a Large Radius Target

$$\langle p \rangle = \frac{1}{n}\int_0^\infty p\ \frac{dn}{dp}\ dp$$

$$= \frac{e^{-\ell/\lambda_\pi}}{n}\sum_{\nu=0}^{\infty}\frac{1}{\nu!}\int_0^\ell \left(\frac{x}{\lambda}\right)^\nu e^{-\frac{x}{\lambda}\left(1-\frac{\lambda}{\lambda_\pi}\right)}\frac{n_\pi^{(\nu)}}{T_\nu}\left(\int_0^\infty p\, e^{-p/T_\nu}\, dp = T_\nu^2\right)\frac{dx}{\lambda}. \tag{27}$$

$$\text{For } T_\nu = \tau_0 (1-K)^{3\nu/4} E_0^{3/4} = \tau_0 \beta^{3\nu} E_0^{3/4}$$

$$\left(n_\pi^{(\nu)} = n_0 \beta^\nu E_0^{1/4}\right)\left(T_\nu = \tau_0 \beta^{3\nu} E_0^{3/4}\right) = n_0\ \tau_0 E_0 \beta^{4\nu}$$

$$\frac{\langle p \rangle}{\tau_0 E_0^{3/4}} = \frac{\beta - \left(1 - \frac{\lambda}{\lambda_\pi}\right)}{(1-K) - \left(1 - \frac{\lambda}{\lambda_\pi}\right)}\ \frac{e^{\frac{\ell}{\lambda}\left[1 - K - \left(1 - \frac{\lambda}{\lambda_\pi}\right)\right]} - 1}{e^{\frac{\ell}{\lambda}\left[\beta - \left(1 - \frac{\lambda}{\lambda_\pi}\right)\right]} - 1} \tag{28}$$

(a) For $\lambda = 2/3\ \lambda_\pi$

$$\frac{\langle p \rangle}{\tau_0 E_0^{3/4}} = (3\beta - 1)\ \frac{e^{\frac{\ell}{3\lambda}} - 1}{e^{\frac{\ell}{\lambda}\left(\beta - \frac{1}{3}\right)} - 1}. \tag{29}$$

(b) For $\lambda = \lambda_\pi$

$$\frac{\langle p \rangle}{\tau_0 E_0^{3/4}} = \frac{\beta}{1 - K} \quad \frac{e^{\frac{\ell}{\lambda}(1 - K)} - 1}{e^{\frac{\ell\beta}{\lambda}} - 1} . \tag{30}$$

These curves are displayed in Fig. 3.

3. Number of Mesons above Momentum p from a Large Radius Target

If one makes the approximation for $T_{(\nu)}$ that appears in the denominator of the exponential of Eq. (20) as follows:

$$T_{(\nu)} \equiv \left(\tau_0 E_0^{3/4} \equiv T_0 \right) \beta^{3\nu},$$

$$\beta \equiv (1 - K)^{1/4}, \tag{31}$$

$$\frac{1}{T_{(\nu)}} \approx \frac{1}{T_0} \left(1 + \frac{3\nu K}{4} \right), \tag{32}$$

$$q \equiv p/T_0, \tag{33}$$

then Eq. (21) can be manipulated into the form of Eq. (22). Integrating (21) from $p' = p$ to $p' = \infty$ one obtains,

$$\frac{n(> q)}{n_0 E_0^{1/4} e^{-q}} = e^{-\ell/\lambda_\pi} \quad \frac{\exp\left\{ \left[\beta\, e^{-3Kq/4} - \left(1 - \frac{\lambda}{\lambda_\pi} \right) \right] \frac{\ell}{\lambda} \right\} - 1}{\beta\, e^{-3Kq/4} - \left(1 - \frac{\lambda}{\lambda_\pi} \right)} . \tag{34}$$

This function is plotted in Fig. 4(a) for $\lambda = \lambda_\pi$ and clearly demonstrates that if one is interested in high-energy mesons for energetic neutrinos, i.e., for $q > 4$, then the optimum target thickness is very nearly one mean free path. The curve for $q = 0$ is the same one already shown in Fig. 3, labeled $\lambda_\pi = \lambda$. Because in our thick-target, large-radius example we have ignored the contributions by mesons that could escape out the edge of a small radius target, all we can say at the moment is that the target thickness for low-energy neutrinos should be greater than $2.6\,\lambda$.

4. Distortion of the Very Thin Target Meson Production Spectrum by a Large-Radius, Thick Target

By making the approximation of Eq. (33) it is possible to obtain the distortion factor,

$$\frac{dn}{dq} \Big/ \left(\frac{dn}{dq}\right)_{\substack{\text{undistorted} \\ \text{very thin target}}} = \left(\frac{\lambda}{\ell}\right) \frac{e^{\frac{\ell}{\lambda} b} - 1}{b} e^{-\frac{\ell}{\lambda_\pi}} \tag{35}$$

$$b \equiv \frac{e^{-3Kq/4} - \beta^2 \left(1 - \frac{\lambda}{\lambda_\pi}\right)}{\beta^2}. \tag{36}$$

For $\ell/\lambda << 1$ this ratio is equal to one. This distortion factor is plotted in Fig. 4(b).

B. Small-Radius Target (Real Targets)

Here, we can not use the assumption that all mesons exit from the end of the target and must use both (a) and (b) parts of Eq. (16).

1. CKP Model Prediction

Figure 5(a) is the analogue of Fig. 4(a) for the quantity $n(>q)/n_0 E^{1/4} e^{-q}$ for a small-radius target. The maximum now occurs at $\ell/\lambda =$. The distortion factors are shown in Fig. 5(b).

2. Other Models

These calculations will be appended to revised versions of this note as they are run on the computer.

C. Upper Limits to the Beam Power Dissipation in Targets

The energy of the nucleon emerging from the target is

$$\langle E \rangle / E_0 = e^{-\ell K/\lambda}, \tag{36a}$$

and of the mesons

$$E_{\text{mesons}} \text{ (lower limit)} = n_0 T_0 E_0 \left(e^{-K\ell/\lambda} - e^{-\ell/\lambda}\right). \tag{36b}$$

Figure 4(c) (right-hand scale) plots the maximum fraction of beam power in the target.

V. A COMPLEX NUCLEUS AS A SPECIAL CASE OF A "THICK TARGET"

The purpose of this discussion is to obtain a qualitative to semi-quantitative estimate of how multiple interactions of a proton within a single nucleus will affect the meson production spectrum.

Equation (25) can be used for this purpose. In our considerations, once a meson interacts within a nucleus it is not considered useful for producing a reasonable energy neutrino. Those same mesons, however, could produce visible charged secondaries emerging from the nucleus, and would be counted as charged secondaries. We ignore them here. Furthermore, we ignore the size of the incident nucleon. Our calculations are, therefore, invalid for the lightest nuclei ($A \lesssim 6$).

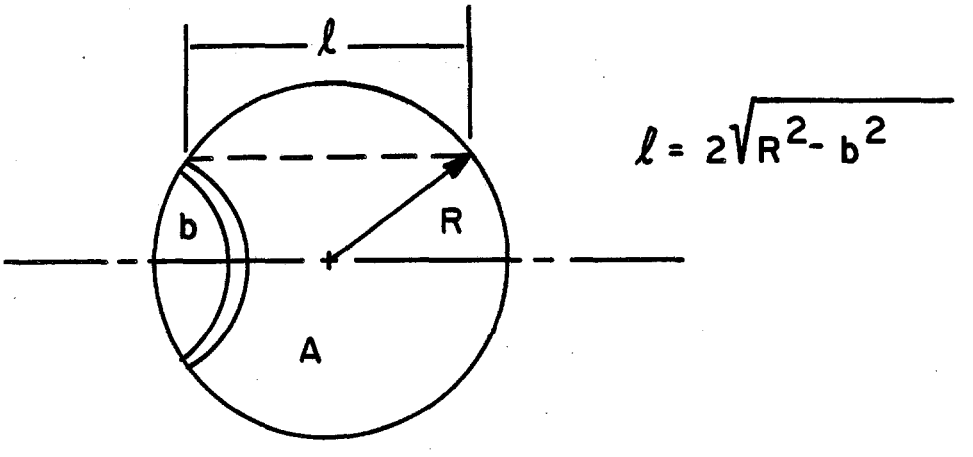

Using Eq. (25) we can write,

$$\frac{\langle\langle n\rangle\rangle}{n_0 E_0^{1/2}} = \frac{1}{\pi R^2}\int_0^R 2\pi b\, db \left(\frac{3}{3\beta - 1}\right)\left[e^{-2(1-\beta)\frac{\sqrt{R^2-b^2}}{\lambda}} - e^{-4\frac{\sqrt{R^2-b^2}}{3\lambda}}\right], \quad (37)$$

$$\frac{\langle\langle n\rangle\rangle}{n_0 E_0^{1/4}} = \frac{6}{3\beta - 1}\left\{\frac{1 - \left[1 + 2(1-\beta)\frac{R}{\lambda}\right]e^{-2(1-\beta)\frac{R}{\lambda}}}{\left[2(1-\beta)\frac{R}{\lambda}\right]^2} - \frac{1 - \left(1 + \frac{4}{3}\frac{R}{\lambda}\right)e^{-\frac{4}{3}\frac{R}{\lambda}}}{\left[\frac{4}{3}\frac{R}{\lambda}\right]^2}\right\}. \quad (38)$$

Using R and λ in "natural units," i.e.,

$$\sigma_{\text{natural}} = \pi R^2 = \pi\left(\frac{\hbar}{m_\pi C}\right)^2 A^{2/3}, \quad (39)$$

$$\text{nuclear density} = A/\frac{4}{3}\pi R^3 N_{av} \quad g/cm^3, \quad (40)$$

$$\lambda = \left[\frac{1}{\pi\left(\frac{\hbar}{m_\pi C}\right)^2 N_{av}}\right] \Big/ (\text{nuclear density}),$$

$$R/\lambda = \frac{3}{4} A^{1/3}. \quad (41)$$

Inserting (41) into (38)

$$\frac{\langle\langle n\rangle\rangle}{n_0 E_0^{1/4}}$$

$$= \left(\frac{6}{3\beta - 1}\right) \left\{ \frac{1 - \left\{1 + \left[\frac{3}{2}(1-\beta)A^{\frac{1}{3}}\right]\right\} e^{-\frac{3}{2}(1-\beta)A^{\frac{1}{3}}}}{\left[\frac{3}{2}(1-\beta)A^{\frac{1}{3}}\right]^2} - \frac{1 - \left(1 + A^{\frac{1}{3}}\right) e^{-A^{\frac{1}{3}}}}{A^{\frac{2}{3}}} \right\} . \quad (42)$$

Figure 6 displays the variation of $\langle\langle n\rangle\rangle / n_0 E_0^{1/4}$ with $A^{1/3}$. It shows a marked resemblance to the corresponding curve ($\lambda_\pi = 3/2\ \lambda$) of Fig. 3. It should be remembered that this calculation is not valid for small A.

The reduction of the mean pion momentum caused by the multiple interaction of the incident nucleon within the nucleus A can be estimated. Using Eqs. (25), (28), and (42) we can write

$$\frac{\langle\langle p\rangle\rangle}{T_0 E^{3/4}}$$

$$= (3\beta - 1) \frac{\left[\frac{1 - \left(1 + \frac{2}{3}\frac{R}{\lambda}\right) e^{-\frac{2}{3}\frac{R}{\lambda}}}{\left(\frac{2}{3}\frac{R}{\lambda}\right)^2} - \frac{1 - \left(1 + \frac{4}{3}\frac{R}{\lambda}\right) e^{-\frac{4R}{\lambda}}}{\left(\frac{4}{3}\frac{R}{\lambda}\right)^2} \right]}{\left\{ \frac{1 - \left[1 + 2(1-\beta)\frac{R}{\lambda}\right] e^{-2(1-\beta)\frac{R}{\lambda}}}{\left[2(1-\beta)\frac{R}{\lambda}\right]^2} - \frac{1 - \left(1 + \frac{4}{3}\frac{R}{\lambda}\right) e^{-\frac{4}{3}\frac{R}{\lambda}}}{\left(\frac{4}{3}\frac{R}{\lambda}\right)^2} \right\}}, \quad (43)$$

which for $R/\lambda = 3/4\ A^{1/3}$, is plotted in Fig. 6. It shows how the average meson momentum is degraded by the multiple nucleon interactions within the complex nucleus. Clearly, the high-energy neutrinos will be diminished by using targets of heavy nuclei.

VI. CONCLUSIONS

For low-energy neutrino physics thick targets will be used. The optimum length will be approximately three mean free paths or more. For these lengths, Fig. 3 shows that the mean meson momentum is ~ two thirds that for a thin target. Pions are the source of low-energy neutrinos and kaons of high-energy ones. The optimum target length for high-energy neutrino physics is one mean free path. How these considerations affect the choice of decay length is summarized in Fig. 7(a). In this figure are plotted optimum decay distances for pions and kaons into two different size detectors, 1.8 meter radius and 1.0 meter radius for accelerator energies from 100 GeV to 500 GeV. These curves were obtained by considering the canonical mesons of the accelerator and a muon shield of 300 meters length. Canonical pions have the same velocity as the incident proton and kaons 2/3 of it. The values of the optimum lengths are obtained from Fig. 5, page 337 of reference 3.* The fraction of the canonical mesons that put neutrinos into the detector are displayed in Fig. 7(b) and are obtained from the

*These curves are reproduced here on graph paper to aid in their use as Figs. 10(a) and 10(b), respectively.

graphs of Fig. 6, page 338 of reference 3.* The decay lengths agree well with the NUFLUX programs for perfect focusing.

In Fig. 7(a) are two energy scales, one for thick targets (pions) contracted by a factor 2/3 from the second one for thin targets (kaons). One can observe the fortuitous situation, namely that what is good for thick-target pions is also good for thin-target kaons. At 200 GeV for a detector of 1 m radius the optimum decay lengths for pions and kaons are 500 m and 400 m, respectively. At 500 GeV these lengths are both 1000 m. Figure 7(b) shows that the detection probability doubles in going from 200 GeV to 500 GeV provided the decay length is changed from 400 m to 1000 m. If the decay length is not changed, but remains at 400 m, a loss of a factor of two occurs for neutrinos above 160 GeV at the 400 GeV. This can be seen in Fig. 2 of reference 4, reproduced here as Fig. 8(a).

Here we encounter a difficult judgment. If neutrino-target stations are expensive (i.e. $\geq$ \$2 m) would NAL be justified in this kind of an expediture for factors of two in rare neutrino flux when at 400 GeV there are already two orders of magnitude difference between low-energy ($E_\nu \sim 10$ GeV) and high-energy ($E_\nu \sim 160$ GeV) flux? Furthermore, uncertainties in productionmechanisms cause a factor of ten uncertainity in absolute flux. See, for example, Fig. 8(b) (a copy of

*These curves are reproduced here on graph paper to aid in their use as Figs. 10(c) and 10(d), respectively.

Fig. 1 of reference 4) which compares the CKP predictions with those of Hagedorn-Ranft shows an order of magnitude difference in the predicted flux. If the shield is shortened to 150 m + 23 m, the optimum lengths shorten somewhat. Figures 9(a) and (b) are analogous to Fig. 7(a) and (b). In coming to a decision it will be helpful to separate those factors which are fairly predictable, e.g., variation of flux as a function of decay length, from those that are not reliably predicted such as the absolute flux.

The system that would best match the flexibility of the accelerator would be a two-phase beam with target station T_{500} to be fully equipped at a later date. Anything that could be done to make the target stations less expensive should be done. According to Maschke[5] the expense

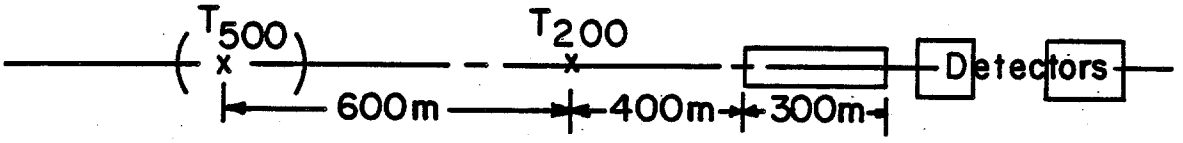

would be least if they were at elevation ≈ 745 ft (about five feet above ground level).

There is an often heard adage--"One should always choose the third best. The best is too expensive; second best takes too long to get. Third best is possible."

Hopefully, the considerations of this paper will assist us in not choosing "fourth best."

REFERENCES

[1] R. K. Adair, Phys. Rev. 172, 1370 (1968).

[2] Y. W. Kang and F. A. Nezrick, Neutrino Beam Design, National Accelerator Laboratory 1969 Summer Study Report SS-146, Vol. I, p. 217.

[3] M. L. Stevenson et al., The Neutrino Facility at NAL, National Accelerator Laboratory 1968 Summer Study Report B. 1-68-104, Vol. I, p. 270.

[4] Y. W. Kang and M. L. Stevenson, Properties of the Neutrino Beams at a 400-GeV Accelerator, National Accelerator Laboratory Internal Report TM-217, February 9, 1970.

[5] A. W. Maschke (National Accelerator Laboratory), personal communication, 1970.

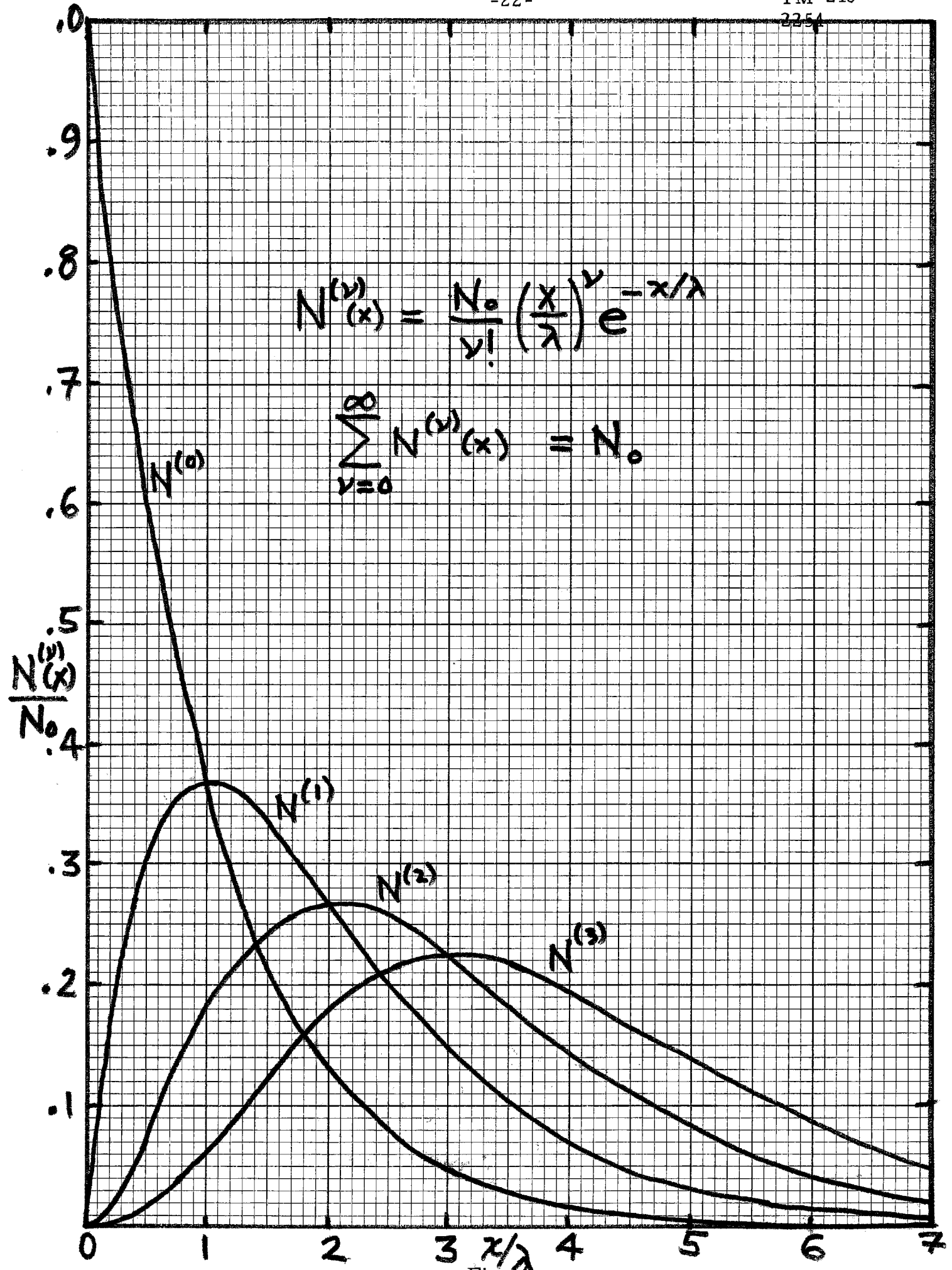
$N^{(\nu)}(x) = \frac{N_0}{\nu!}\left(\frac{x}{\lambda}\right)^{\nu} e^{-x/\lambda}$
$\sum_{\nu=0}^{\infty} N^{(\nu)}(x) = N_0$
$N^{(0)}$
$N^{(1)}$
$N^{(2)}$
$N^{(3)}$
$\frac{N^{(\nu)}(x)}{N_0}$
.0
.9
.8
.7
.6
.5
.4
.3
.2
.1
0
1
2
3
4
5
6
7
x/λ

Fig. 1

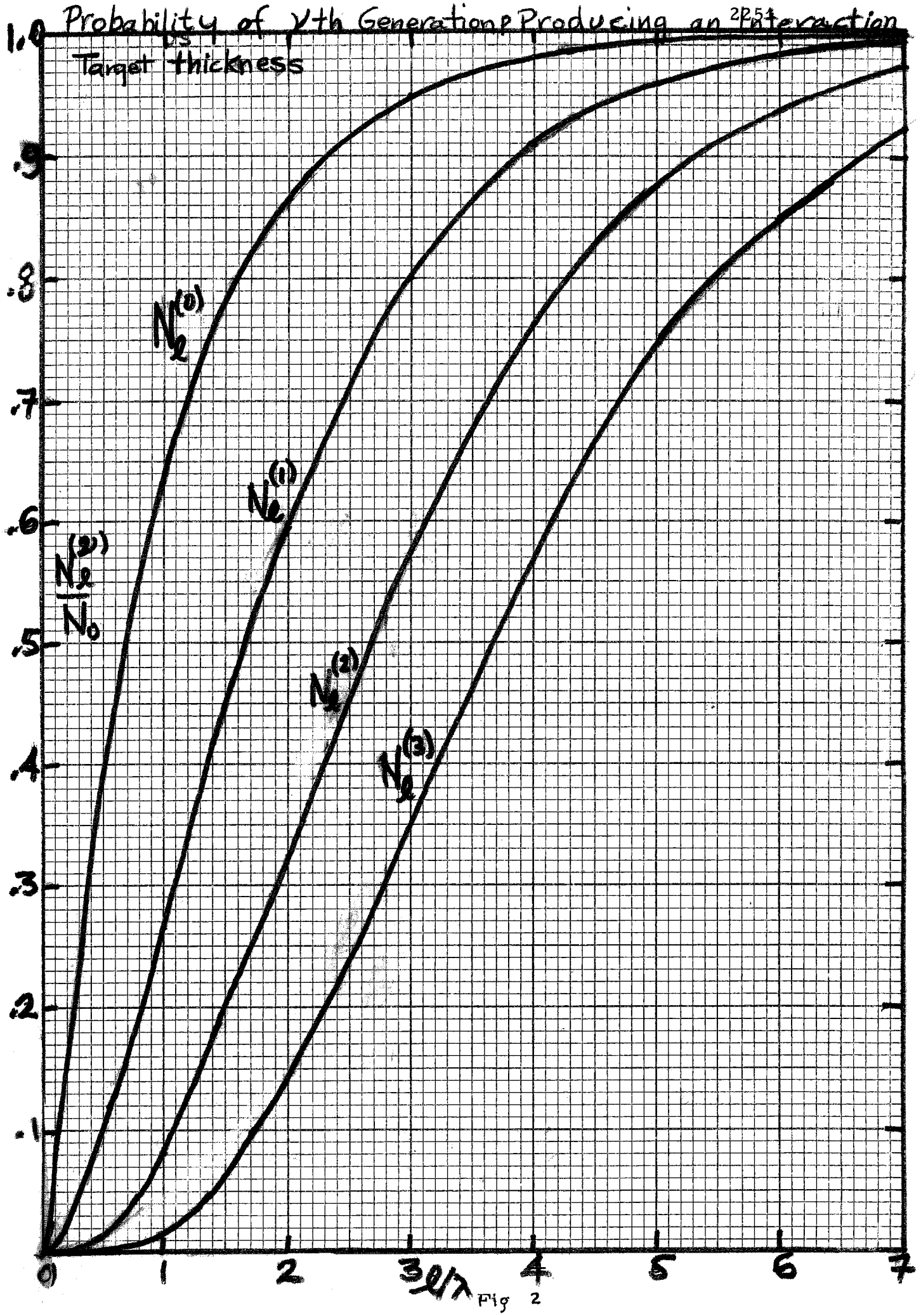
Probability of νth Generation Producing an Interaction
vs
Target thickness
1.0
.9
.8
.7
.6
.5
.4
.3
.2
.1
$N_\ell^{(0)}$
$N_\ell^{(1)}$
$N_\ell^{(2)}$
$N_\ell^{(3)}$
$\frac{N_\ell^{(\nu)}}{N_0}$
0
1
2
3
4
5
6
7
ℓ/λ

Fig 2

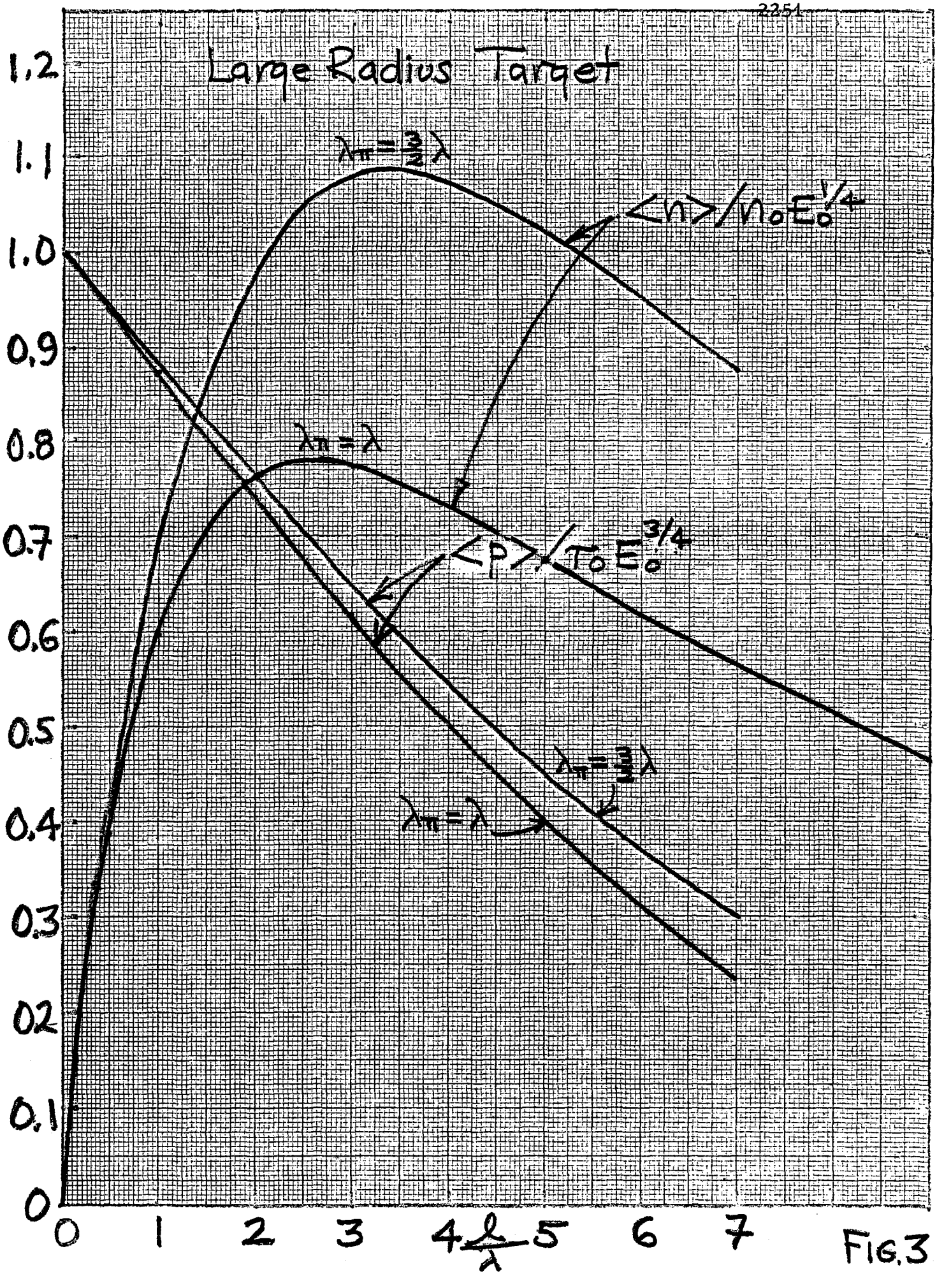
Large Radius Target
$\lambda_\pi = \frac{3}{2}\lambda$
$\langle n \rangle / n_0 E_0^{1/4}$
$\lambda_n = \lambda$
$\langle P \rangle / T_0 E_0^{3/4}$
$\lambda_\pi = \frac{3}{2}\lambda$
$\lambda_\pi = \lambda$
1.2
1.1
1.0
0.9
0.8
0.7
0.6
0.5
0.4
0.3
0.2
0.1
0
0 1 2 3 4 5 6 7
$\frac{\ell}{\lambda}$

FIG. 3

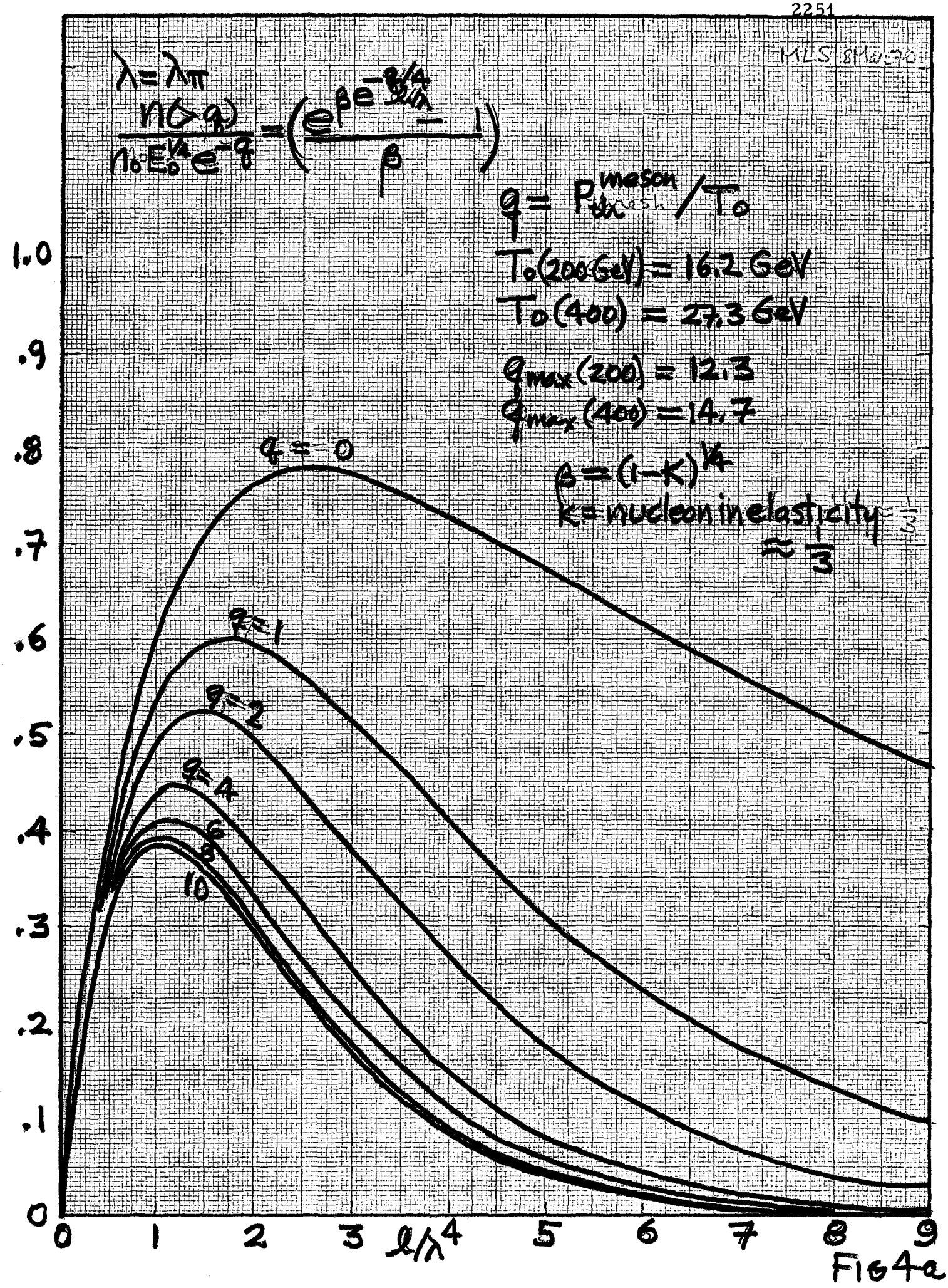
MLS 8/20/70
$\lambda = \lambda_\pi$
$\frac{n(>q)}{n_0 E_0^{1/4} e^{-q}} = \left(\frac{e^{\beta e^{-q/\lambda}} - 1}{\beta}\right)$
$q = P_{lab}^{meson} / T_0$
$T_0(200\,GeV) = 16.2\,GeV$
$T_0(400) = 27.36\,eV$
$q_{max}(200) = 12.3$
$q_{max}(400) = 14.7$
$\beta = (1-K)^{1/4}$
K = nucleon inelasticity $\approx \frac{1}{3}$
q = 0
q = 1
q = 2
q = 4
6
8
10
1.0
.9
.8
.7
.6
.5
.4
.3
.2
.1
0
0 1 2 3 l/λ^4 5 6 7 8 9

Fig 4a

$$\frac{dn}{dq}\Big/\left(\frac{dn}{dq}\right)_{\substack{\text{undistorted}\\ \text{very thin target}}} = \left(\frac{\lambda}{\ell}\right)\frac{e^{\ell/\lambda b}-1}{b}\,e^{-\ell/\lambda_\pi}$$

$$b \equiv \frac{e^{-3Kq/4} - \beta\left(1-\frac{\lambda}{\lambda_\pi}\right)}{\beta^2}$$

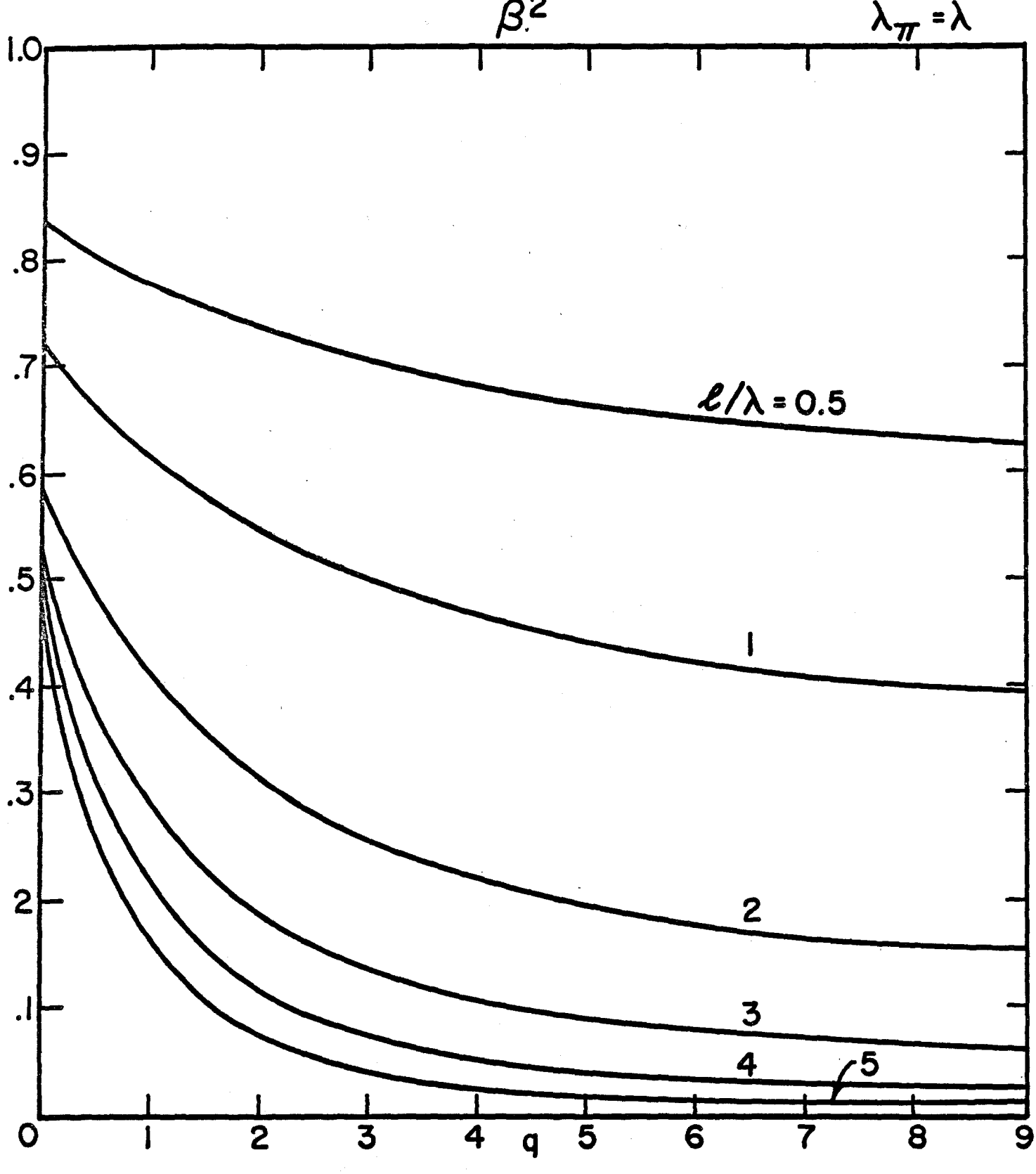

Fig. 4(b)

16 Mar 70
MCS

Fraction of Beam Power that Leaves the End of a Large Radius Target.

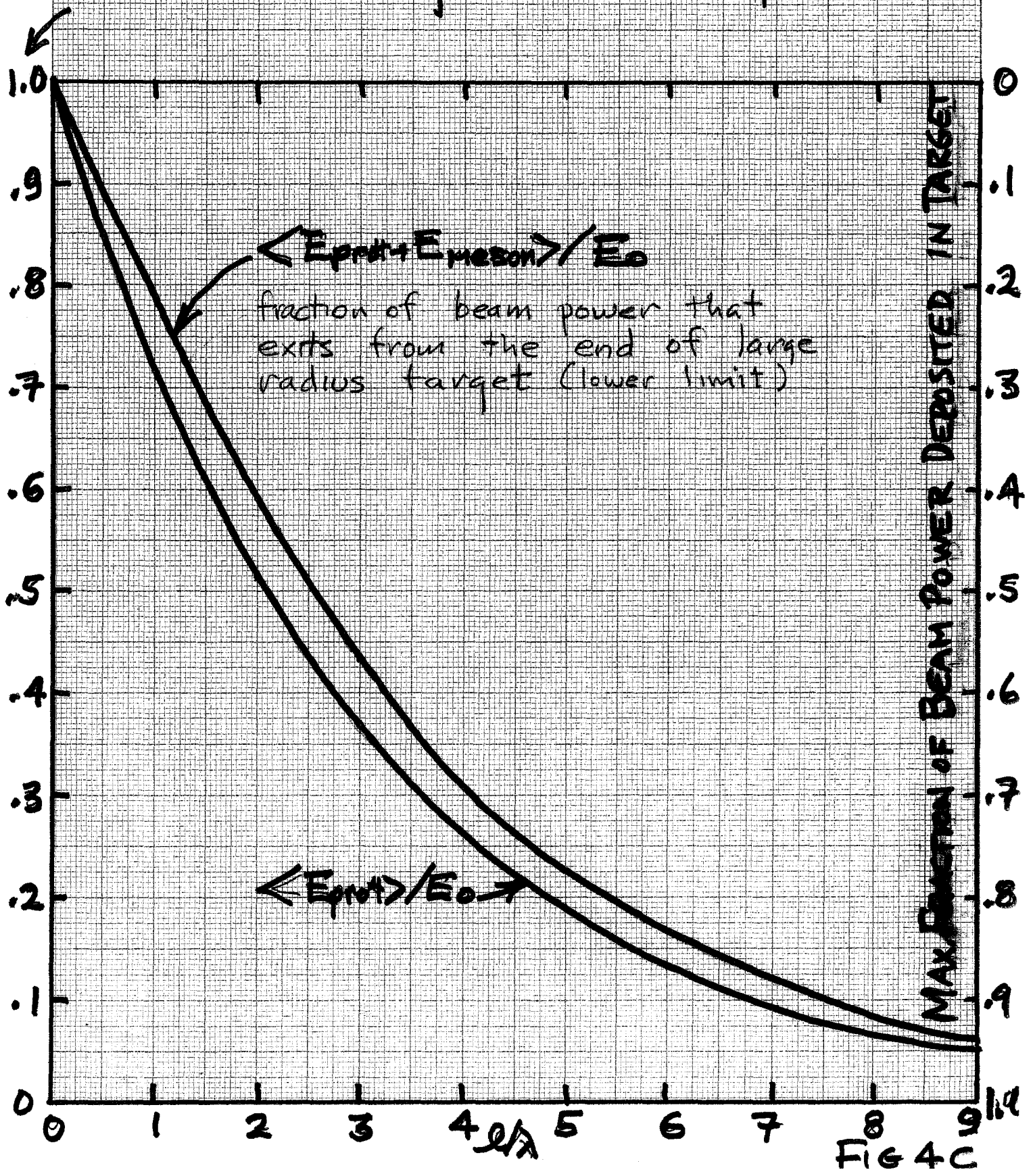

Fig 4C

Small Radius Target

$n(>q)/n_0 E_0^{1/4} E^{-q}$ vs e/λ

for $q = 0$
1
2
.
.
.
10.

Fig 5a

Small Radius Target

$dn/dq / (dN/dq)_{very\ thin}$

Fig 5b

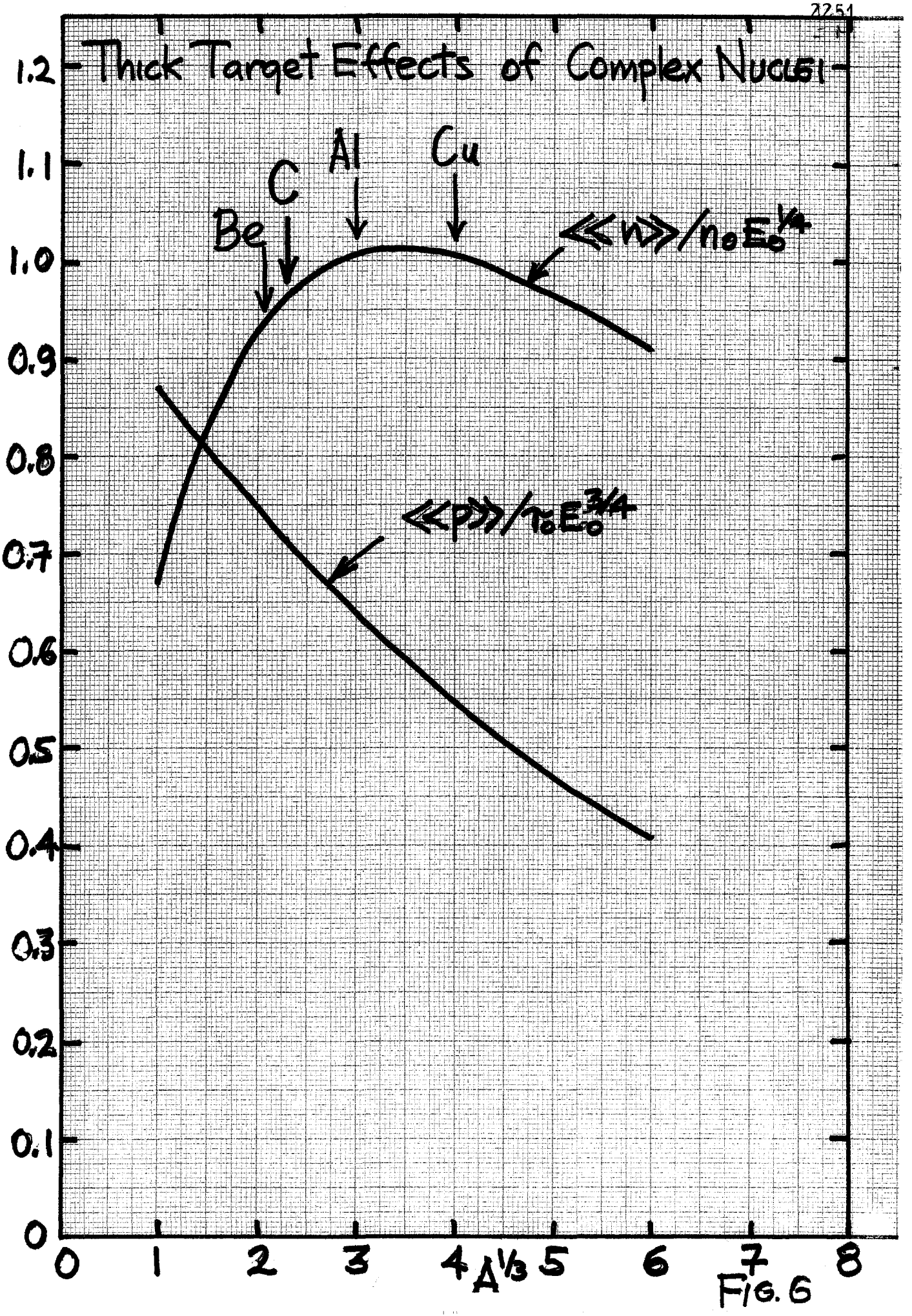
Thick Target Effects of Complex Nuclei
Be
C
Al
Cu
≪w≫/n₀E₀^1/4
≪p≫/n₀E₀^3/4
1.2
1.1
1.0
0.9
0.8
0.7
0.6
0.5
0.4
0.3
0.2
0.1
0
0
1
2
3
4
5
6
7
8
A^1/3

FIG. 6

10 Mar 70
MLS

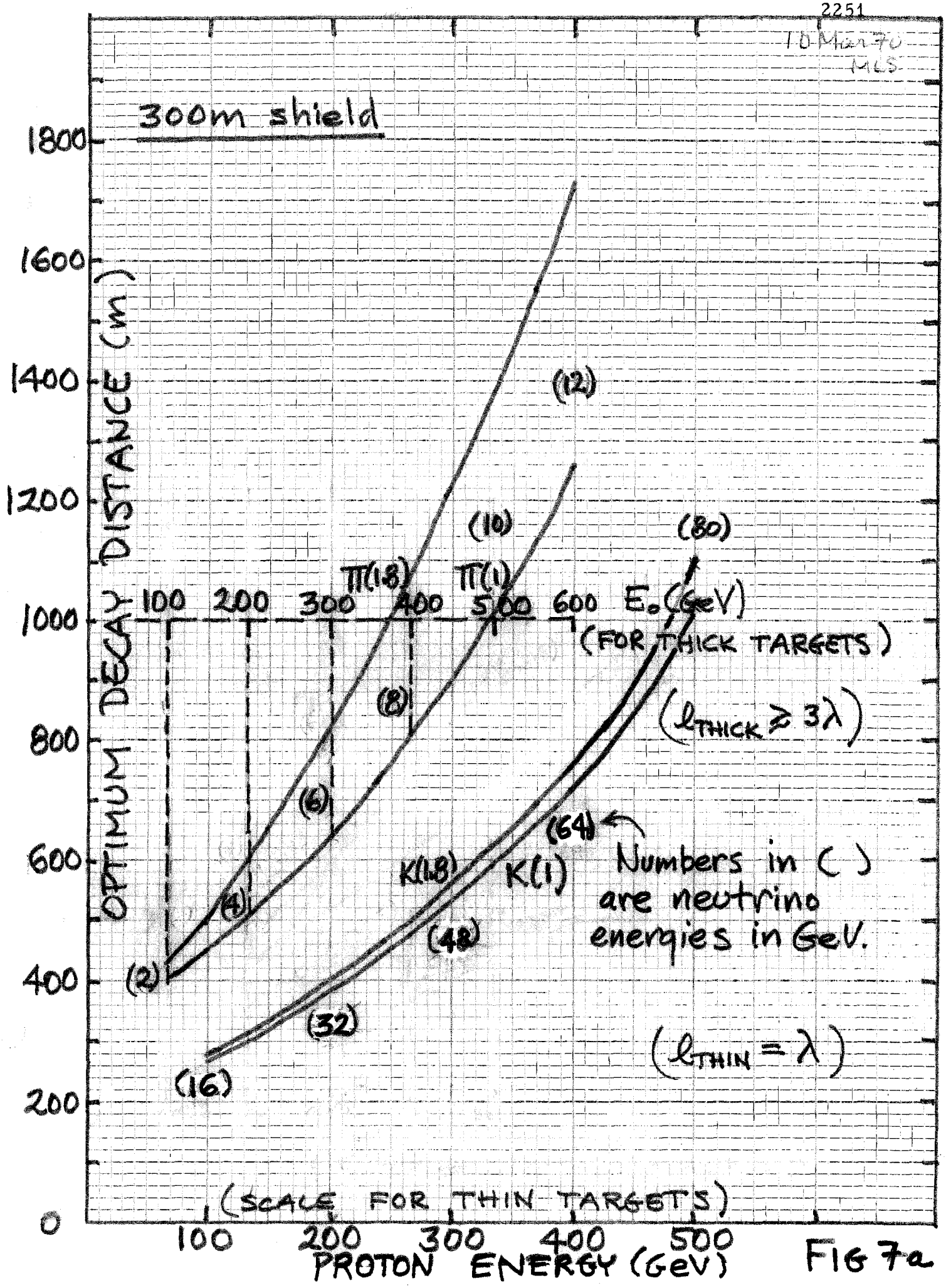

FIG 7a

11 Mar 70
MCS

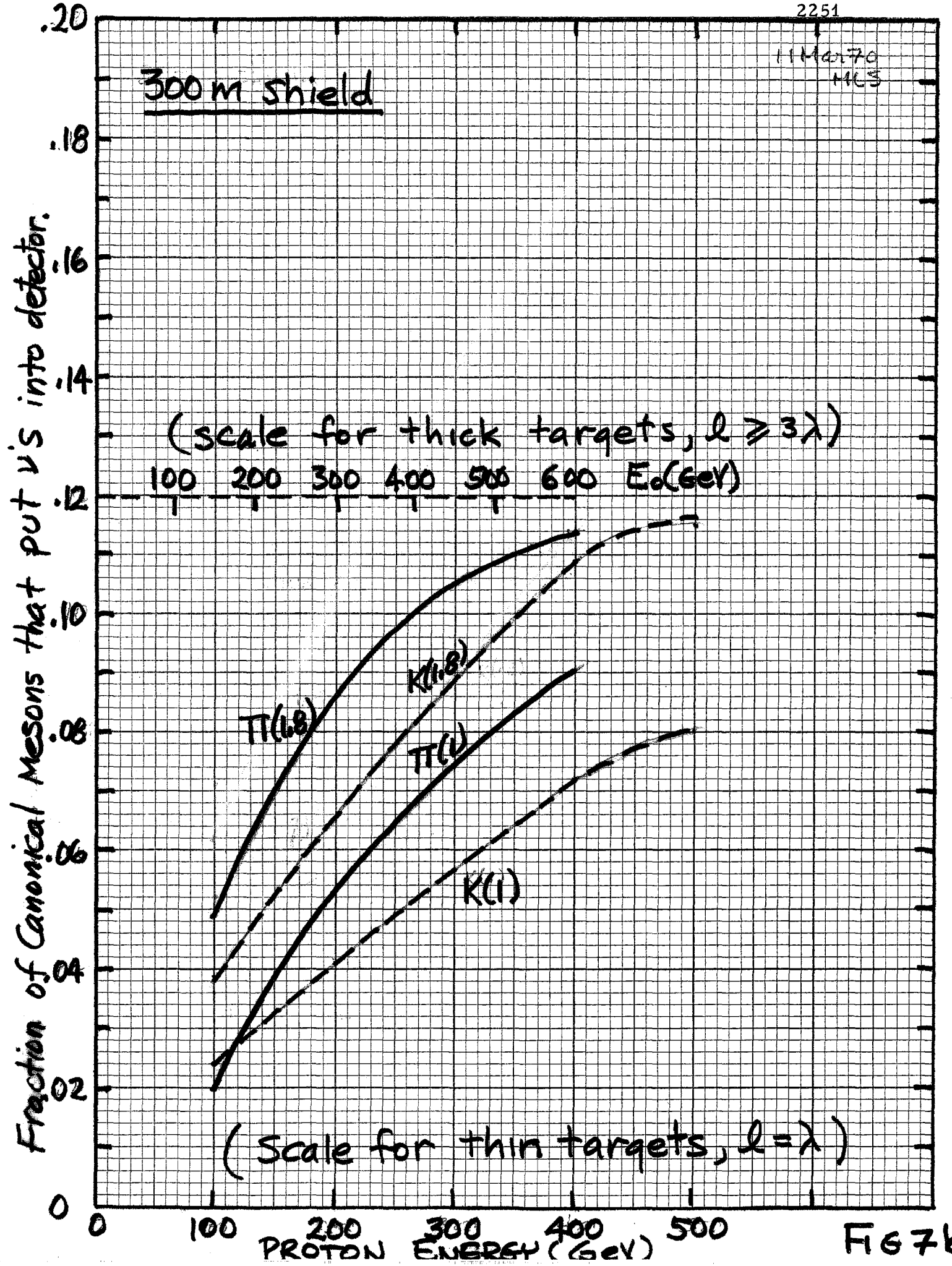

Fig 7b

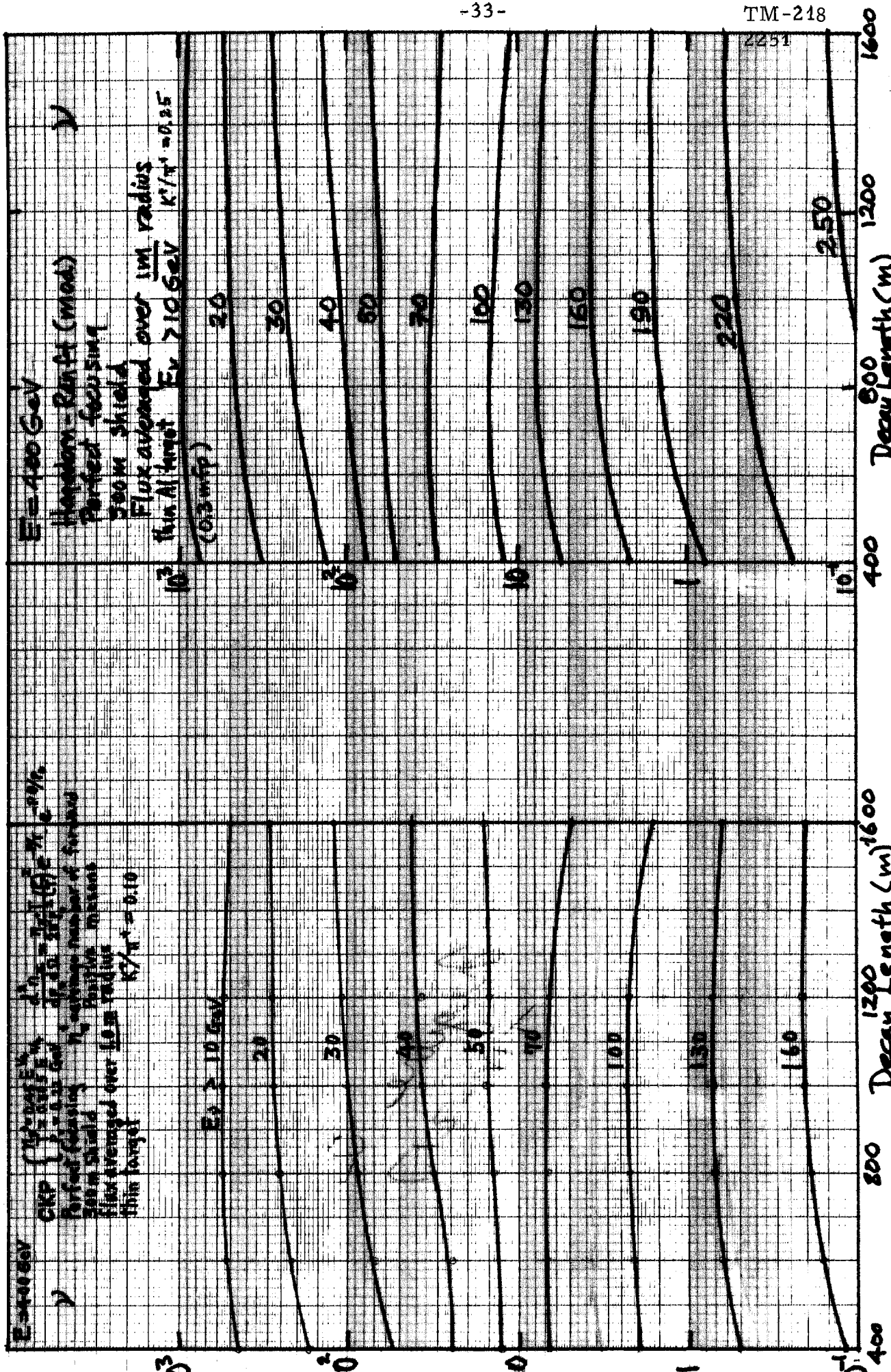
Number of μ's above Eμ/10⁶ incident protons/m²
Decay Length (m)
E = 400 GeV
Hadron-Beryl (mod)
Perfect focusing
200m shield
Flux averaged over 1m radius
Eμ > 10 GeV
K⁺/π⁺ = 0.25
thin Al target
(0.3 mfp)
2.0
3.0
4.0
60
70
100
130
160
190
220
250
Energy GeV
CKP
Perfect focusing
200m shield
Flux averaged over 10m radius
thin target
K/π⁺ = 0.10
E₀ > 10 GeV
20
30
40
50
70
100
130
160

Fig. 8(a)

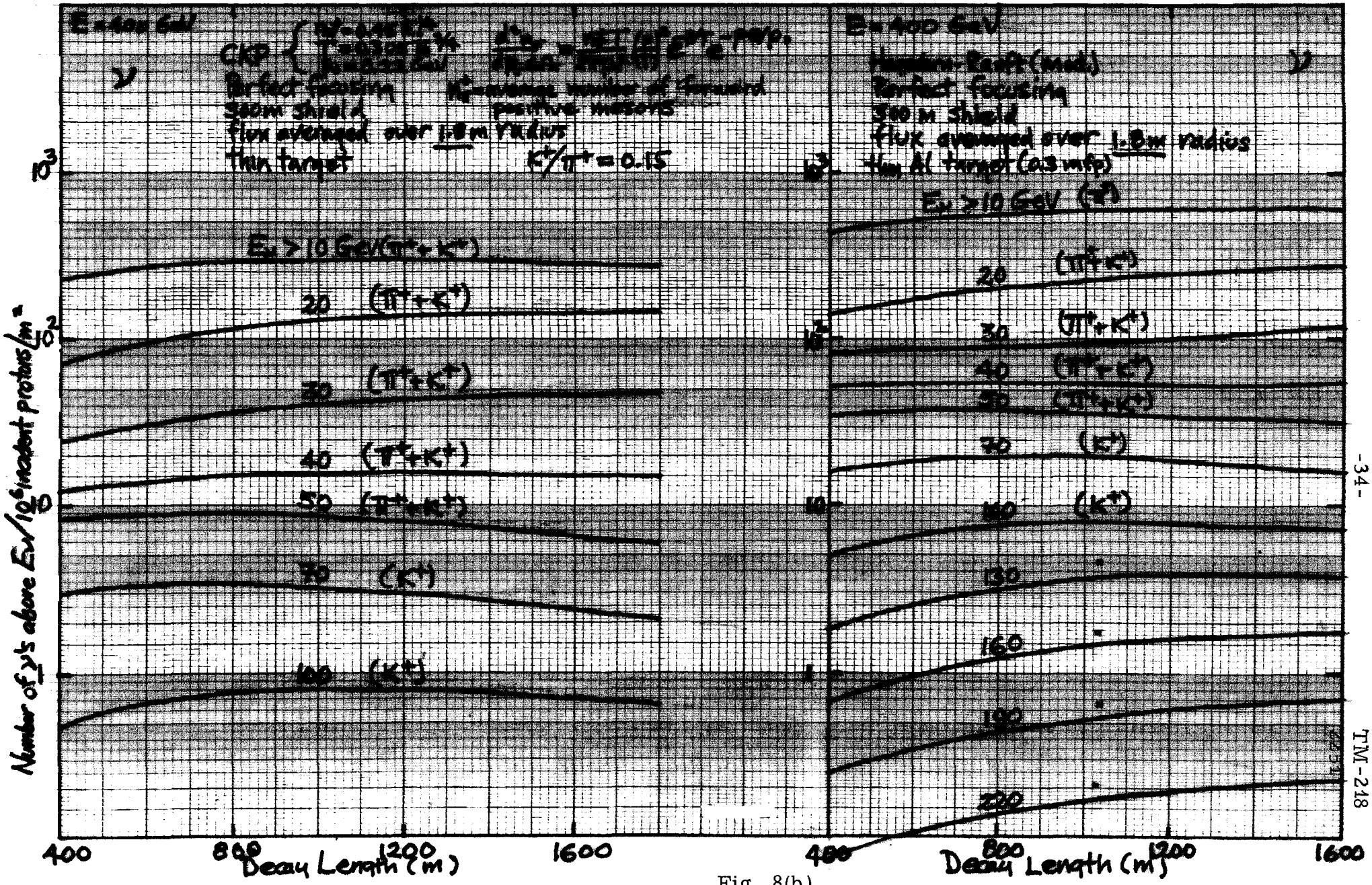
E = 400 GeV
ν
Perfect focusing
300m shield
flux averaged over 1.8m radius
thin target
K+/π+ = 0.15
E = 400 GeV
ν̄
Perfect focusing
300 m shield
flux averaged over 1.8m radius
Eν ≥ 10 GeV (π+)
20 (π+ + K+)
30 (π+ + K+)
40 (π+ + K+)
50 (π+ + K+)
30 (K+)
100 (K+)
Eν ≥ 10 GeV (π+ + K+)
20 (π+ + K+)
30 (π+ + K+)
40 (π+ + K+)
50 (π+ + K+)
30 (K+)
100 (K+)
130
160
190
220
Number of ν's above Eν/10^6 incident protons/m^2
Decay Length (m)
400
800
1200
1600

Fig. 8(b)

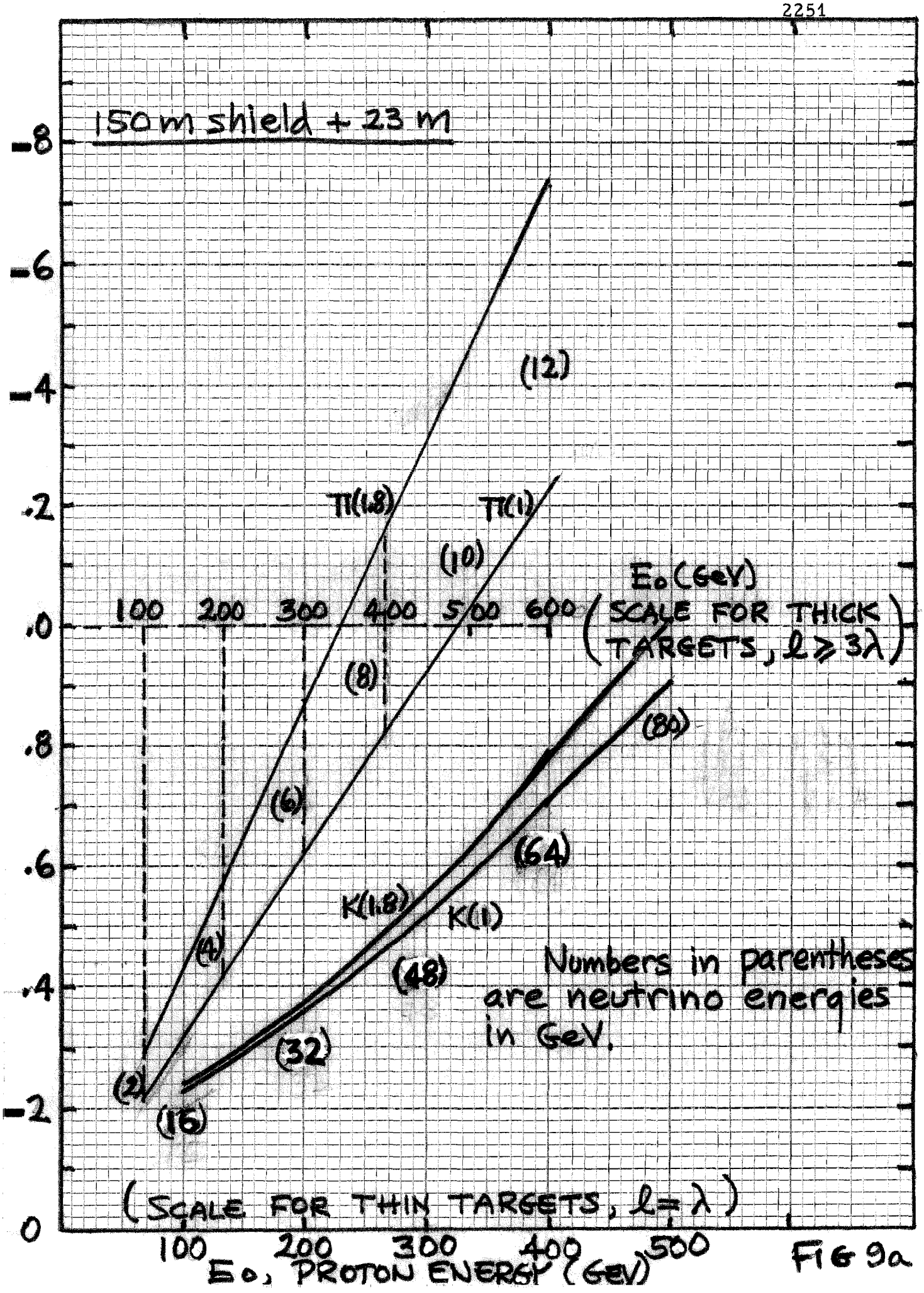
150 m shield + 23 m
-8
-6
-4
-2
.2
.0
.8
.6
.4
0
100
200
300
400
500
600
E₀ (GeV)
(SCALE FOR THICK TARGETS, ℓ ≥ 3λ)
(SCALE FOR THIN TARGETS, ℓ = λ)
E₀, PROTON ENERGY (GeV)
π(1.8)
π(1)
K(1.8)
K(1)
(2)
(4)
(6)
(8)
(10)
(12)
(16)
(32)
(48)
(64)
(80)
Numbers in parentheses are neutrino energies in GeV.

Fig 9a

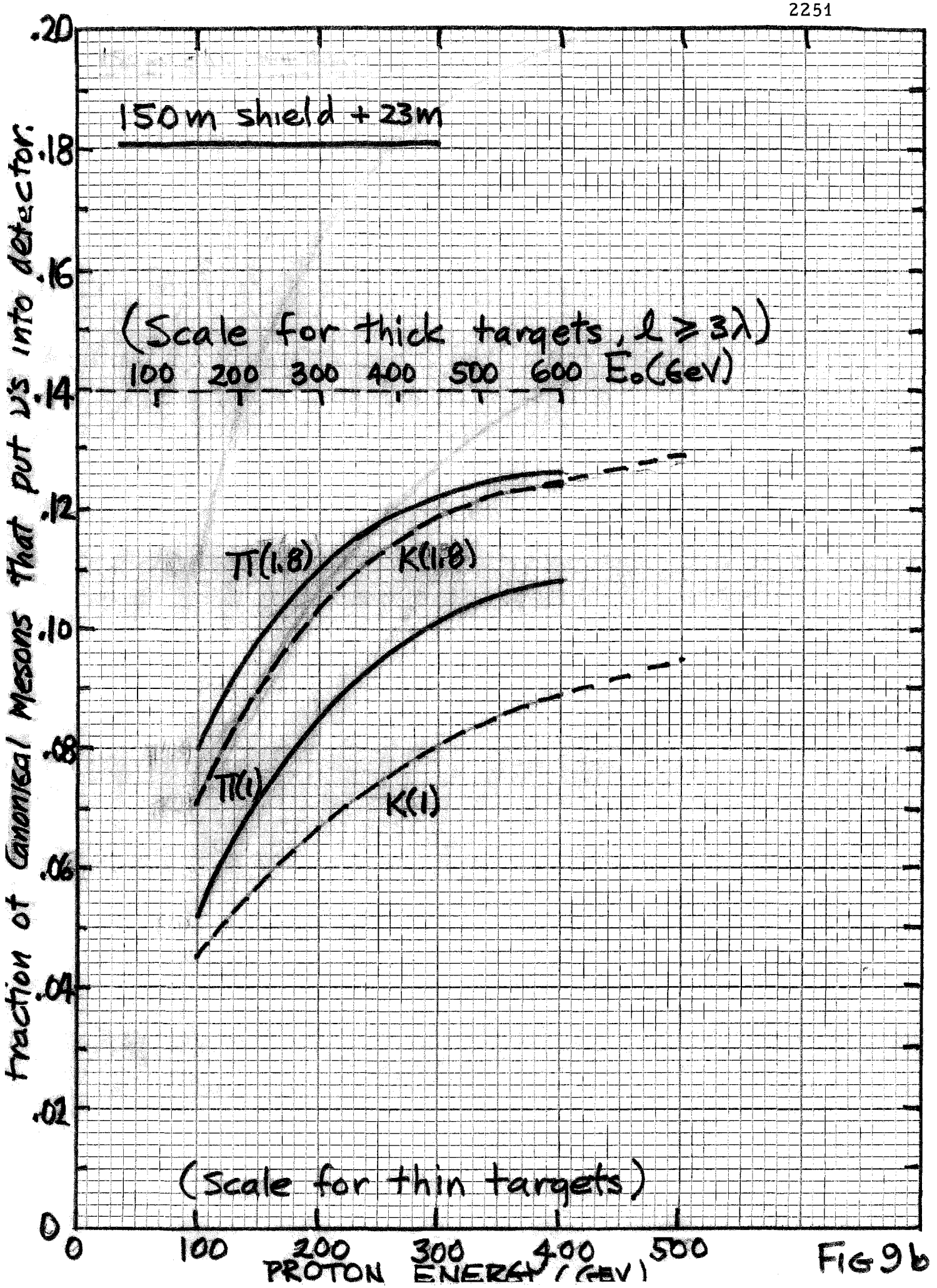
150m shield + 23m
(Scale for thick targets, $\ell \geq 3\lambda$)
100 200 300 400 500 600 E_o(GeV)
π(1.8)
K(1.8)
π(1)
K(1)
(Scale for thin targets)
Fraction of Canonical Mesons that put ν's into detector.
.20
.18
.16
.14
.12
.10
.08
.06
.04
.02
0
0
100
200
300
400
500
PROTON ENERGY (GEV)

Fig 9b

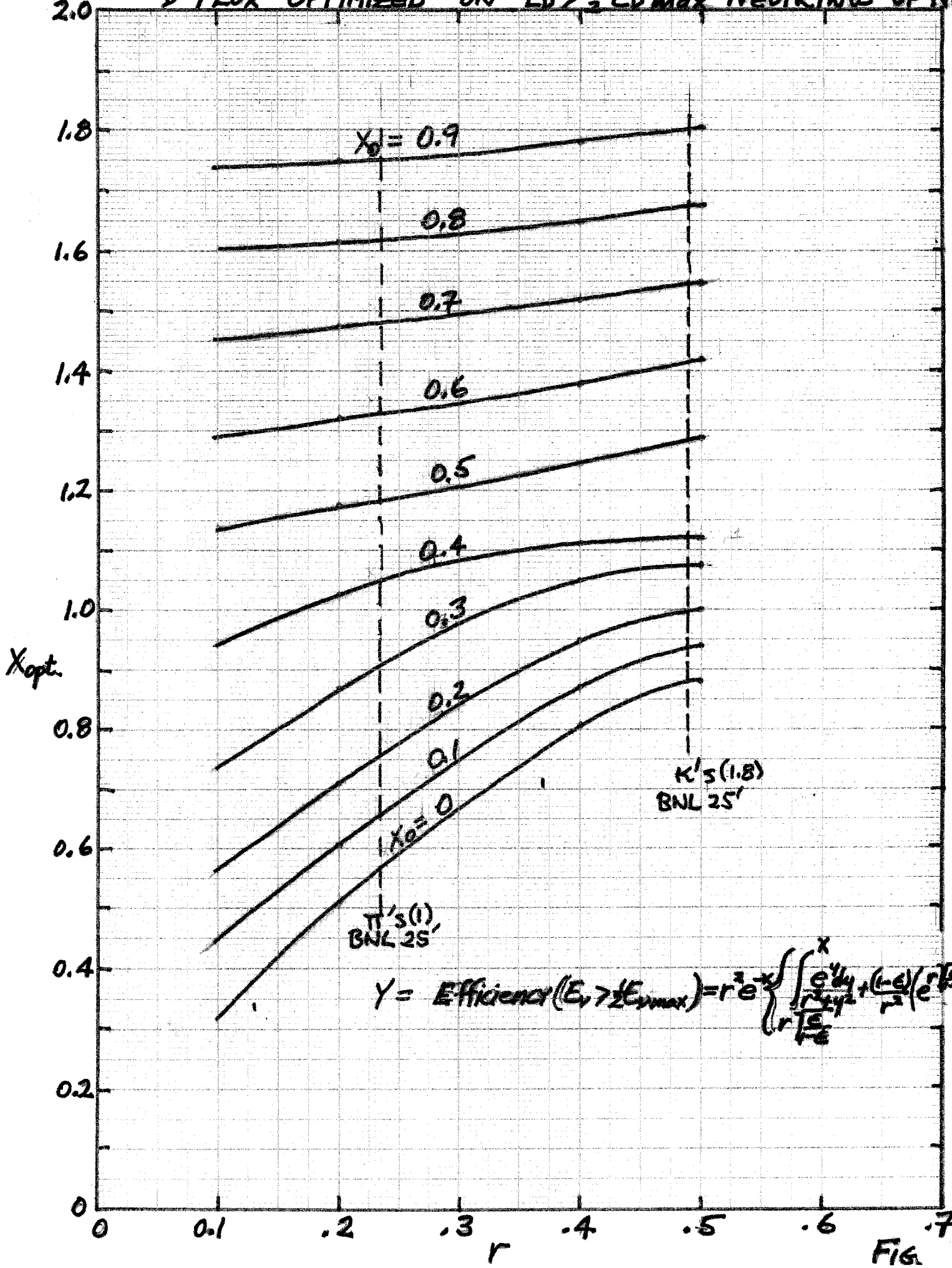
ν FLUX OPTIMIZED ON $E_\nu > \frac{1}{2} E_{\nu max}$ NEUTRINOS OF NBS
$X_0 = 0.9$
0.8
0.7
0.6
0.5
0.4
0.3
0.2
0.1
$X_0 = 0$
$X_{opt.}$
$K's(1.8)$
BNL 25'
$\pi's(1)$
BNL 25'
$Y = \text{Efficiency}(E_\nu > \frac{1}{2} E_{\nu max}) = r^3 e^{-x} \left\{ \int_{r\sqrt{\frac{\epsilon}{1+\epsilon}}}^{x} \frac{e^{y} dy}{r^2 + y^2} + \frac{(1-\epsilon)}{r^2} \left(e^{r\sqrt{\frac{\epsilon}{1+\epsilon}}} - e^{x} \right) \right.$
0
0.1
.2
.3
.4
.5
.6
.7
r
1.0
0.8
0.6
0.4
0.2
1.2
1.4
1.6
1.8
2.0

FIG. 100

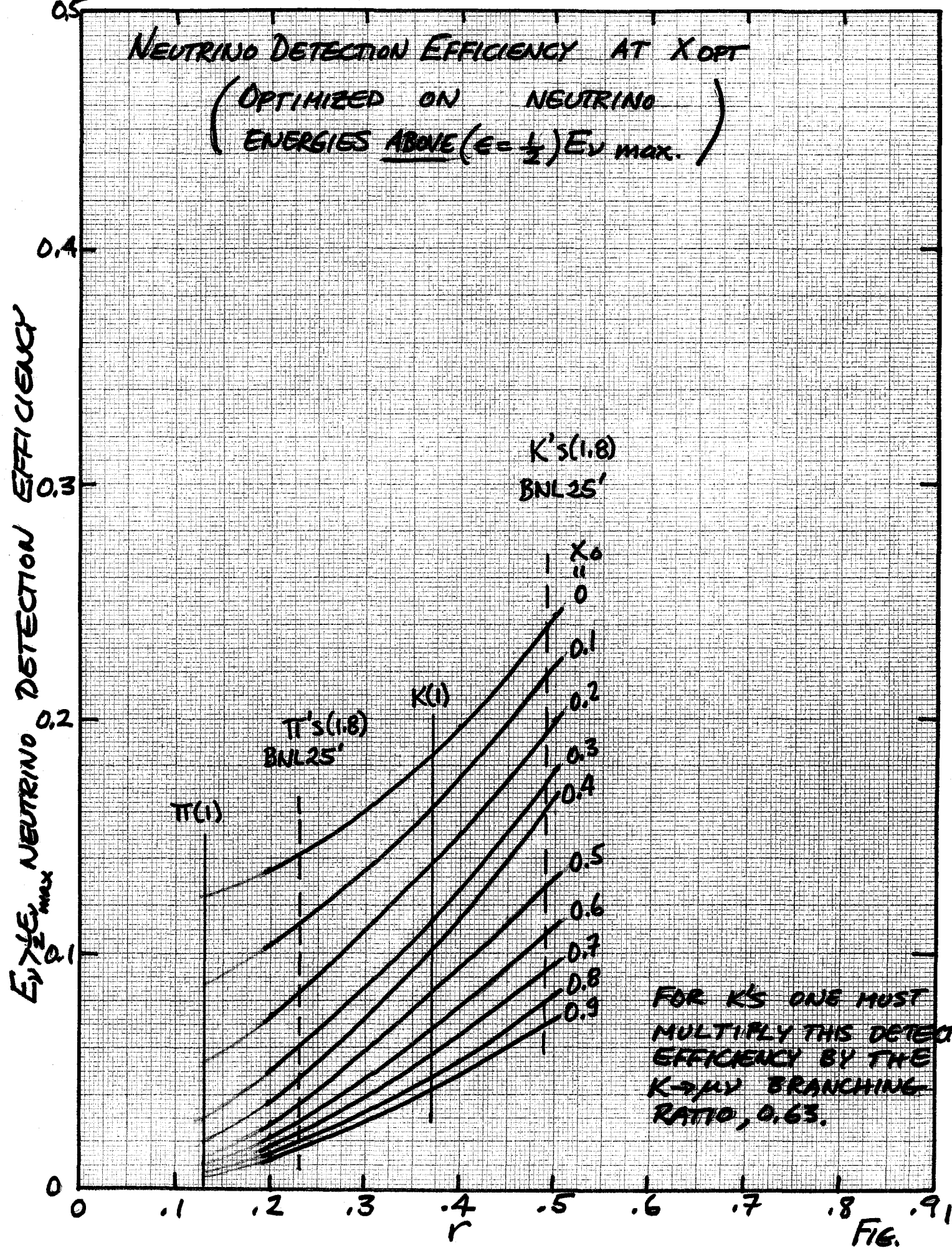
NEUTRINO DETECTION EFFICIENCY AT X OPT
(OPTIMIZED ON NEUTRINO ENERGIES ABOVE (ε = ½) Eν max.)
Eν > ½ Eν max NEUTRINO DETECTION EFFICIENCY
0.5
0.4
0.3
0.2
0.1
0
K's(1.8)
BNL25'
X0 =
0
0.1
0.2
0.3
0.4
0.5
0.6
0.7
0.8
0.9
K(1)
π's(1.8)
BNL25'
π(1)
FOR K's ONE MUST MULTIPLY THIS DETECTION EFFICIENCY BY THE K→μν BRANCHING RATIO, 0.63.
0
.1
.2
.3
.4
.5
.6
.7
.8
.9
r
10b

FIG.

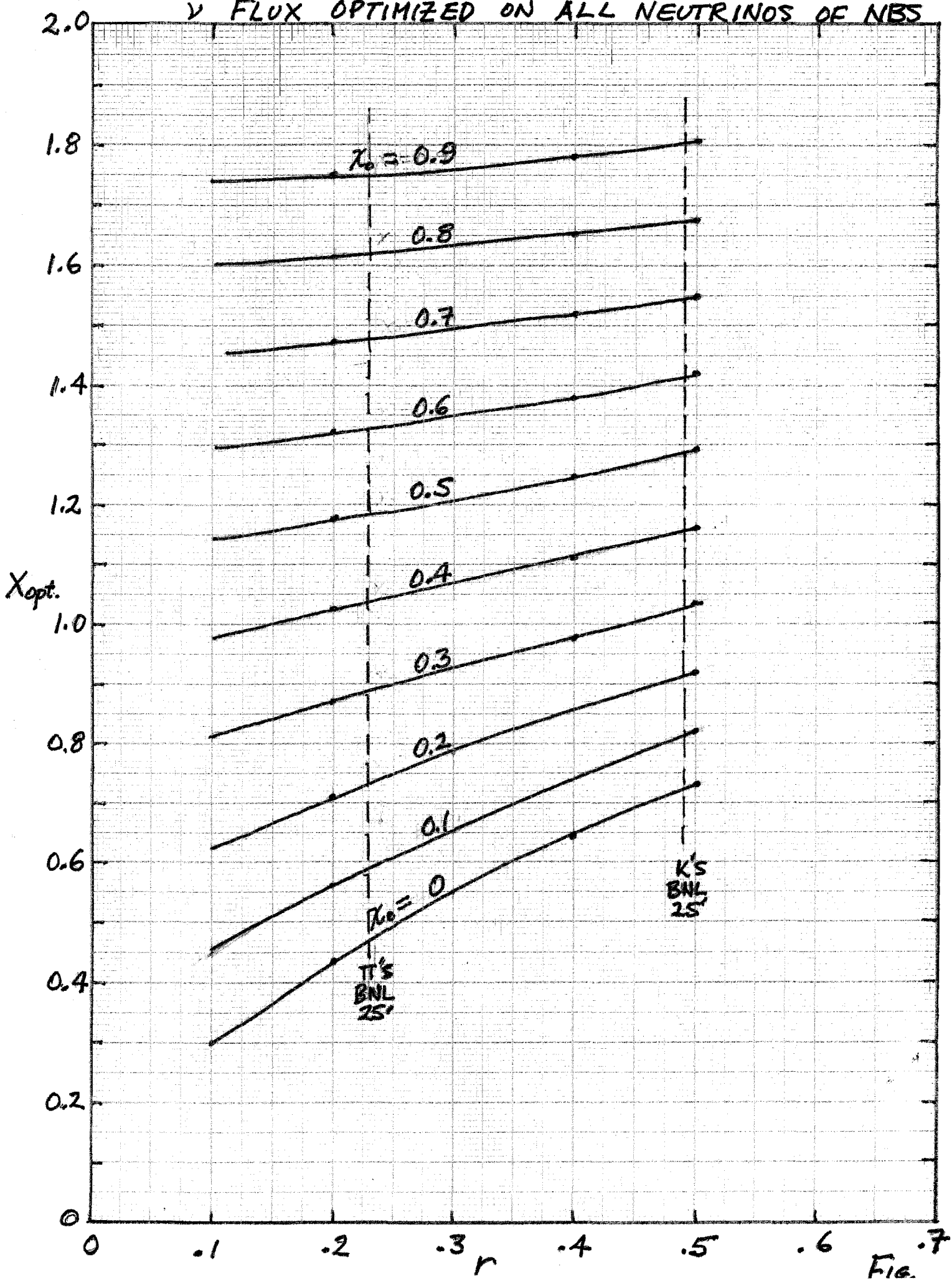
ν FLUX OPTIMIZED ON ALL NEUTRINOS OF NBS
$X_{opt.}$
r
$\chi_0 = 0.9$
0.8
0.7
0.6
0.5
0.4
0.3
0.2
0.1
$\chi_0 = 0$
K's BNL 25'
π's BNL 25'
2.0
1.8
1.6
1.4
1.2
1.0
0.8
0.6
0.4
0.2
0
.1
.2
.3
.4
.5
.6
.7

Fig. 10c

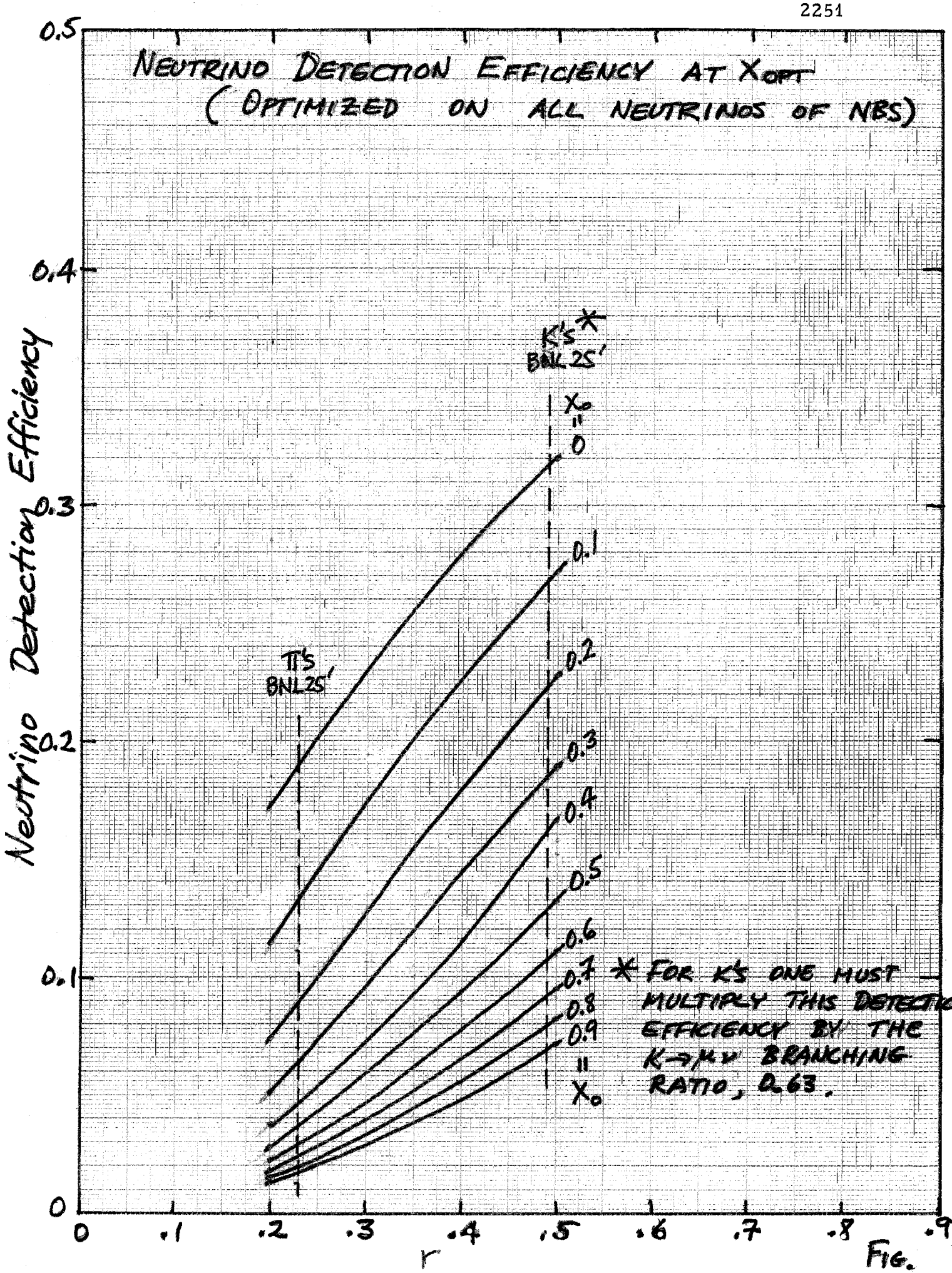
NEUTRINO DETECTION EFFICIENCY AT X_{OPT}
(OPTIMIZED ON ALL NEUTRINOS OF NBS)
Neutrino Detection Efficiency
0.5
0.4
0.3
0.2
0.1
0
K's* BNL 25'
T's BNL 25'
X_0 = 0
0.1
0.2
0.3
0.4
0.5
0.6
0.7
0.8
0.9
11 X_0
* FOR K's ONE MUST MULTIPLY THIS DETECTION EFFICIENCY BY THE $K \to \mu\nu$ BRANCHING RATIO, 0.63.
0 .1 .2 .3 .4 .5 .6 .7 .8 .9
r
10d

FIG.